arTs Università degli Studi di Trieste
Archivio della ricerca – postprint

Study of gain, noise, and collection efficiency of GaAs SAM-APDs single pixel

M. Colja,[a,*] M. Cautero,[a] R.H. Menk,[b,c,d] P. Palestri,[e] A. Gianoncelli,[b] M. Antonelli,[c] G. Biasiol,[f] S.D. Zilio,[f] T. Steinhartova,[f] C. Nichetti,[g] F. Arfelli,[c,g] D. De Angelis,[b] F. Driussi,[e] V. Bonanni,[b] A. Pilotto,[e] G. Gariani,[b] S. Carrato[a] and G. Cautero[b,c]

[a] *Department of Engineering and Architecture, University of Trieste, via Alfonso Valerio 6/1, 34127 Trieste, Italy*

[b] *Elettra-Sincrotrone Trieste S.C.p.A., strada statale 14 - km 163,5 in Area Science Park, 34149 Trieste, Italy*

[c] *Istituto Nazionale di Fisica Nucleare Sezione di Trieste, via Alfonso Valerio 2, 34127 Trieste, Italy*

[d] *Department of Medical Imaging, University of Saskatchewan, 103 Hospital Drive, Saskatoon, SK S7N 5A2, Canada*

[e] *Polytechnic Department of Engineering and Architecture, University of Udine, via delle Scienze 206, 33100 Udine, Italy*

[f] *Laboratorio TASC, Consiglio Nazionale delle Ricerche - Istituto Officina dei Materiali, strada statale 14 - km 163,5 in Area Science Park, 34149 Trieste, Italy*

[g] *Department of Physics, University of Trieste, via Alfonso Valerio 2, 34127 Trieste, Italy*

E-mail: matija.colja@elettra.eu

Abstract: III-V-compound semiconductors offer many advantages over silicon-based technologies traditionally used in solid-state photodetectors, especially in hard X-ray applications that require high detection efficiency and short response times. Amongst them, gallium arsenide (GaAs) has very promising characteristics in terms of X-ray absorption and high carrier velocity. Furthermore, implementing charge-multiplication mechanisms within the sensor may become of critical importance in cases where the photogenerated signal needs an intrinsic amplification before being acquired by the front-end electronics. This work reports on the experimental characterization by means of lasers and synchrotron radiation of gain, noise, and charge collection efficiencies of GaAs avalanche photodiodes (APDs), realized by molecular beam epitaxy (MBE), featuring separate absorption and multiplication regions (SAM) and different absorption region thicknesses.

*Corresponding author.

These devices have been fabricated to investigate the role of the thickness of the absorption region and of possible traps or defects at the metal-semiconductor interfaces in the collection efficiency in order to lay the groundwork for the future development of thicker GaAs devices for detection of hard X-rays.

Keywords: Solid state detectors; X-ray detectors; Detector modelling and simulations II (electric fields, charge transport, multiplication and induction, pulse formation, electron emission, etc)

1 Introduction

Semiconductor-based single-photon detectors typically exploit the avalanche effect in reverse-biased junctions to amplify the photogenerated carriers and improve the signal-to-noise ratio, thus allowing the detection of extremely weak signals. In the visible frequency range, silicon APDs are widely used, however their absorption decreases rapidly for shorter wavelengths (<1 nm), i.e., in the X-ray region, since X-ray absorption scales with a high power of the atomic number limiting the use Si-APDs in medium to hard X-ray experiments.

Compared to silicon devices, III-V compound semiconductors, such as GaAs, have some unique properties, such as a higher density, atomic number and electron mobility, which result in higher detection efficiency and shorter response times. Thanks to these characteristics, in recent years, GaAs, as well as wide-band gap materials such as CVD diamond [1, 2] and SiC [3] have been studied as Si alternatives for the production of X-ray detectors.

The multiplication process is an advantage over the non-multiplicative charge collection as long as the noise induced by the multiplication, represented through the excess noise factor (ENF), is kept low. With APDs, there are two main contributions to such noise: the possibility of the multiplicative process starting in random areas and the occurrence of multiplication for both electrons and holes with similar probabilities, as it happens in GaAs based APD [4]. For these reasons, state-of-the-art devices are characterised by two important properties: a separation between the photon-electron conversion region (absorption layer, ideally immune from multiplication events) and the multiplication region; a superlattice structure of the multiplication layers that results in a staircase profile of the conduction band, which promotes only electron impact ionizations at discrete locations [5]. Devices fabricated with these features are then called *separate absorption and multiplication APDs* (SAM-APDs) [5, 6].

The GaAs SAM-APDs presented in this work were expressly fabricated to lay the groundwork for the subsequent development of hard X-ray detectors and for investigating some important phenomena that are critical as the device becomes thicker.

The results of the measurements carried out with both conventional and synchrotron light sources are reported and discussed in comparison to simulations performed alongside.

2 Materials and methods

2.1 Description of devices and multiplication process

The photogenerated current in the GaAs APD for an incident photon flux Φ_0 (in units [1/s]) of monoenergetic X-rays with energy E_γ can be expressed as

$$I(E_\gamma) = \Phi_0 \cdot \frac{E_\gamma}{E_{\mathrm{e-h}}} \cdot q \cdot QE \cdot \epsilon \cdot M, \tag{2.1}$$

where q is the electron charge, $E_{\mathrm{e-h}} = 4.2\,\mathrm{eV}$ is the average energy required to create an electron/hole pair in GaAs [7], QE is the quantum efficiency, ϵ denotes the charge collection efficiency, and M is the internal avalanche multiplication. Excess multiplication noise results from the stochastic nature of the impact ionisation process that amplifies the photogenerated current [7]. The ENF is defined as the ratio between the actual noise of the APD current and the noise of a device with noiseless multiplication. Then the ENF can be expressed as [7]

$$\mathrm{ENF} = \frac{\mathrm{var}(n)}{M^2 \cdot \mathrm{var}(a)}, \tag{2.2}$$

where n is the number of multiplied output carriers originating from a primary carriers generated by a Poisson process. The ENF in APDs is particularly high when electron and hole ionisation coefficients are very similar, which is exactly the case for GaAs [8]. For this reason, by exploiting of band gap engineering, we fabricated APD devices featuring multiplication layers based on a GaAs/AlGaAs superlattice staircase structure (figure 1) which increases the difference between the effective ionisation coefficients of holes and electrons, dramatically reducing the ENF [7].

The presence of a separate absorption region of a specific thickness ensures that most of the photons (below a given energy) are absorbed within such a layer. The presence of a separation layer between the two regions, under the form of a *p-doped δ layer*, introduces a potential barrier such that, when a reverse bias is applied, the electric field is entirely confined in the multiplication region. As the bias increases, the potential barrier decreases, increasing the photocurrent, and the bias at which the barrier disappears is called the punch-through voltage.

2.2 Device growth and fabrication

For the study at hand, several GaAs APDs have been grown by MBE on a 500 μm-thick heavily Si-doped (2×10^{18} cm^{-3}) n-type GaAs (001) substrate and subsequently patterned into 200 μm-wide mesa structures, following the procedure outlined in [9]. The resulting layered structure is reported in figure 1.

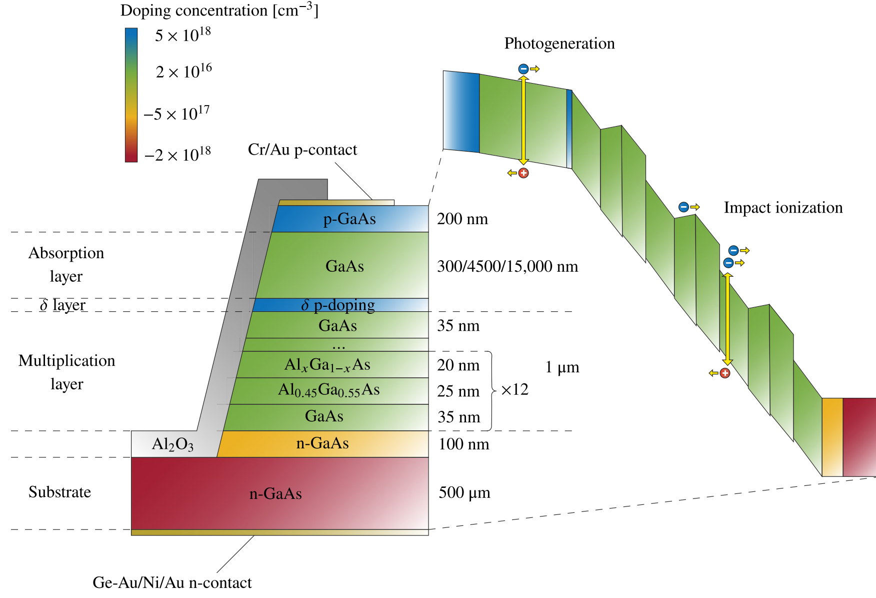

Figure 1. Sketch of the GaAs APD considered in this work (not to scale). The grown layered structure is depicted on the left side. The right side sketches the corresponding band diagram under reverse bias.

Above the p-doped δ layer, three different thicknesses ($d_{\rm abs}$ = 0.3 μm, 4.5 μm, or 15 μm) of intrinsic GaAs were deposited, determining three different types of devices. In order to examine whether the presence of any traps in the metal-semiconductor interface plays a significant role in lowering efficiency, a top Cr-Au contact layer was grown in a way to cover only a portion of the entrance window, so that photons could impinge either onto the gold contact or directly onto the GaAs.

2.3 Simulations and measurement setup

Sentaurus TCAD software suite [10] was used to reproduce the experimental capacitance versus bias, as well as the dark current under different bias conditions. Capacitance measurements were performed by using a high-precision LCR meter (HP4284A, Keysight Technology), whereas a custom-made trans-impendance amplifier was employed to perform current measurements.

The ENF value was measured starting from equation (2.2) where the term var(n), which represents the variance of the multiplied output carriers, can be obtained by integrating the current spectral density S_i over a bandwidth B. Then the ENF can be calculated measuring the spectral density S_i, rewriting equation (2.2) in the following operative form:

$$\mathrm{ENF} = \frac{S_i \cdot B}{M^2 \cdot 2qI_{\rm ph} \cdot B}, \tag{2.3}$$

where $I_{\rm ph}$ is the DC value of the photogenerated current without multiplication.

In order to evaluate the role of the thickness of the absorption region in the charge loss, measurements were carried out with synchrotron light on Twinmic [11] beamline at Elettra Sincrotrone Trieste which can generate a sub-micrometric monochromatic pencil beam in the energy range

between 400 and 2200 eV, where the GaAs attenuation length varies significantly. Five distinct photon energies were chosen (940, 1090, 1500, 1705, and 2010 eV) in order to tune the depth at which the e-h pairs are generated, which depends on the associated attenuation lengths (respectively, 860 nm, 1.2 µm, 360 nm, 450 nm and 680 nm). Therefore, if defects in the absorption region were responsible for a reduction of the collection efficiency, the latter would also change with the attenuation length.

To analyse the effect of the metal-semiconductor interface, we measured the currents when the radiation entered the device, passing exclusively either through the surface covered by the contact or directly in the GaAs. Two-dimensional mesh scans of X-ray fluorescence spectra were preliminarily performed to chemically characterize them.

3 Results

3.1 Capacitance and I-V curves

In figure 2(a), we show the measured and simulated capacitance as a function of the reverse bias. At low biases, a first decrease in capacitance can be observed for all curves, corresponding to the depletion of the multiplication layer. The obtained values are in good agreement with the theoretical capacitance for a parallel-plate capacitor (see the horizontal dashed line in figure 2(a)) featuring an area of $A = \pi\ (100\,\mu\text{m})^2$ and separation of $d = 1\,\mu\text{m}$ (thickness of the multiplication region).

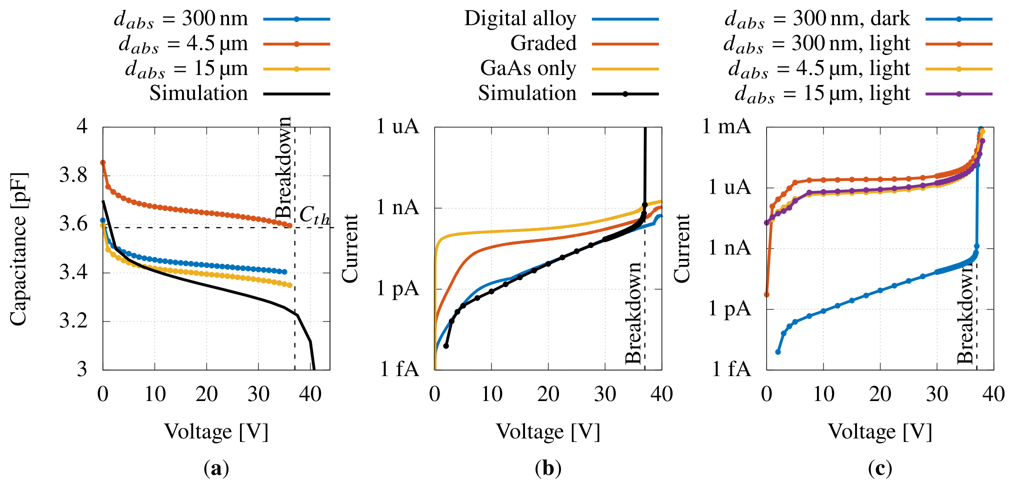

Figure 2. (a) Comparison between measured and simulated C-V curves of devices with different absorption region thicknesses and theoretical capacitance ($C_{\text{th}} = 3.59$ pF) of a parallel-plate capacitor. (b) Dark I-V curves obtained with different models of the multiplication region. (c) Light I–V measurements of the three types of devices.

For the devices analysed in this work, the punch-through is never reached, thus the capacitance remains almost constant up to the breakdown voltage and its value depends practically only on the thickness of the multiplication region (which is the same in all devices).

Figure 2(b) shows the simulated dark current of the device employing different models of the multiplication region. The digital alloy model, in which the graded $Al_xGa_{1-x}As$ layers were modelled with progressively increasing thickness of $Al_{0.45}Ga_{0.55}As$ layers, thus closely reproducing the grown structure [9], provides the best results predicting accurately the experimental data. A typical dark current I–V curve is depicted as a black solid line in figure 2(b) and as a blue solid line in figure 2(c).

The I–V curves of the three types of devices, which were irradiated with the same laser power ($P_{\text{laser}} \approx 50\,\mu$W, $\lambda = 532$ nm), are shown in figure 2(c). For all devices, three distinct regions can be distinguished: firstly, in the reverse-bias range from about 5 to 25 V, an exponential current increase is observable. This exponential trend is consistent with a progressive lowering of the potential barrier of the δ layer. Then, from 25 to about 37 V, a further increase due to multiplication is visible (in light conditions only), and eventually breakdown occurs for voltages above 37 V.

3.2 Excess noise factor

Figure 3(a) reports typical spectra acquired under laser light. At low frequencies, a typical $1/f$ noise is visible, therefore we considered the flat bandwidth region from 1.5 to 2 MHz to estimate the S_i required in equation (2.3).

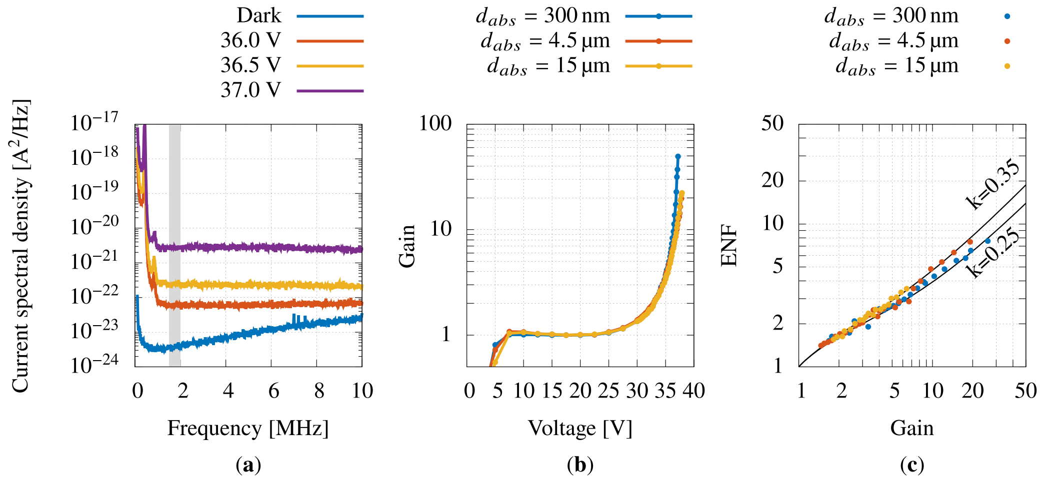

Figure 3. (a) Noise spectra acquired at different biases. The gray-shaded band shows the frequency range used for ENF estimation. (b) Gains as a function of reverse bias. (c) ENF for the three device types compared with the theoretical trend [12] with $k = 0.25$ and $k = 0.35$.

The gains obtained with each type of device, which are necessary in order to compute the ENF, are reported in figure 3(b). For each device type, the S_i were measured and the resulting ENFs are reported in figure 3(c).

It is common to compare the results with the simple local model proposed in [12]: the ENF may be written in terms of both the gain M and the ratio of the ionisation coefficients for electrons and holes, namely $k = \alpha/\beta$. This relation can be expressed in the form [12]

$$\mathrm{ENF}(M) = k \cdot M + (1-k)\left(2 - \frac{1}{M}\right). \tag{3.1}$$

A value of k ranging from 0.25 to 0.35, compared with the one found in simple GaAs PIN diodes, which approximately equals 1 [13], indicates that the staircase structure is effectively hindering the contribution of holes in the avalanche process which implies, from equation (3.1), a reduction of the ENF.

3.3 Synchrotron radiation measurements

The initial X-ray fluorescence scans were used to identify areas that were then used for all subsequent measurements (see marked areas in figure 4).

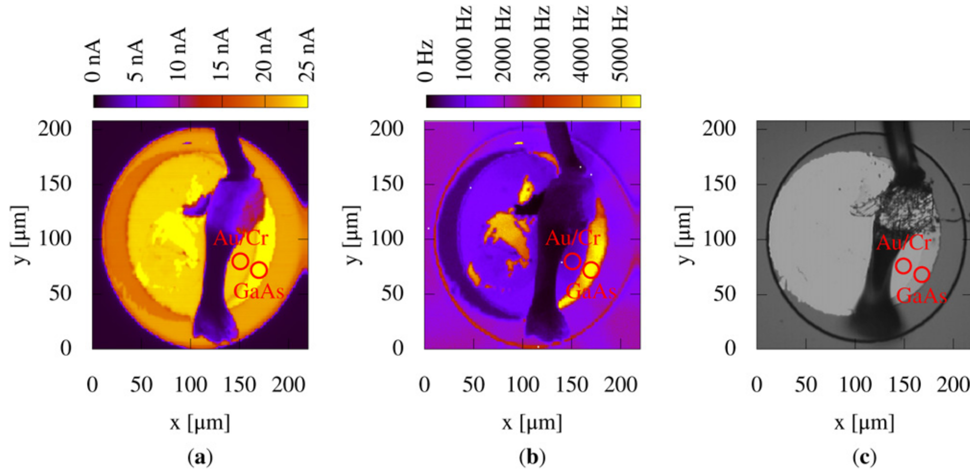

Figure 4. (a) Photocurrent map; (b) X-ray fluorescence image of the As L_α line; (c) optical microscope image of the device. Regions of higher intensities correspond to the unexposed half-moon shaped area of the devices, which are clearly visible in all three images.

The ratio between the current acquired passing through the double metal layer and the one acquired by irradiating directly the GaAs was compared with the theoretical value considering the absorption of Au and Cr. The obtained values are comparable and show a similar trend, indicating that traps and defects between Au/Cr and GaAs surfaces seem to have small effects in the loss of charge collection efficiency.

Since in thicker devices ($d_{\mathrm{abs}} = 4.5$ µm and $d_{\mathrm{abs}} = 15$ µm) at all considered energies, the photons were almost completely absorbed before reaching the multiplication layer, the theoretically expected current (in lossless and gainless devices) could be calculated, considering the photon energy E_{ph} and the incident radiation flux Φ_0 as

$$I_{\mathrm{th}}(E_{\mathrm{ph}}) = \Phi_0 \cdot \frac{E_{\mathrm{ph}}}{E_{\mathrm{e-h}}} \cdot q, \tag{3.2}$$

where $E_{\text{e-h}}$ and q are introduced in equation (2.1). The measured current was compared with the current from equation (3.2) as a function of Φ_0 and E_{ph} so that the efficiency η was calculated as $I_m^{\text{GaAs}}/I_{\text{th}}$.

In figure 5, we report the change in efficiency as the attenuation length increases. There is no clear dependence on the attenuation length for both detectors, therefore there is a negligible carrier recombination in the absorption region. The modest variations between one energy and another are most likely due to systematic errors since, at each change of energy, it was necessary to reposition the sample.

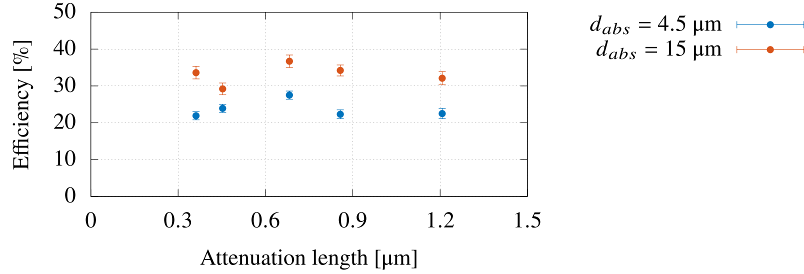

Figure 5. Efficiency as a function of attenuation length.

4 Conclusions

GaAs-based APDs are a valid alternative to Si-based devices thanks to higher atomic number, electron mobility and band-gap energy. Three different types of GaAs SAM-APDs with different absorption layer widths were fabricated and characterized by means of laser and synchrotron radiation. Both recombination in the metal-semiconductor interface and recombination in the absorption region were investigated. The acquired data highlight the absence of traps in the interfacial regions and an independence of the charge collection efficiency from the thickness of the absorption region. These results suggest that it is possible to increase the thickness of the absorption region without severe drawbacks and therefore thicker devices will be fabricated for hard X-rays applications. Furthermore, the measurements confirmed that the ENF can be greatly reduced by implementing a superlattice staircase structure in the multiplication region.

References

[1] S. Bacher et al., *Performance of the diamond-based beam-loss monitor system of Belle II*, *Nucl. Instrum. Meth. A* **997** (2021) 165157.

[2] M. Di Fraia et al., *Fast beam monitor diamond-based devices for VUV and X-ray synchrotron radiation applications*, *J. Synchrot. Radiat.* **26** (2019) 386.

[3] S. Zhao, T. Gohil, G. Lioliou and A.M. Barnett, *Soft X-ray detection and photon counting spectroscopy with commercial 4H-SiC Schottky photodiodes*, *Nucl. Instrum. Meth. A* **830** (2016) 1.

[4] G.E. Bulman, V.M. Robbins, K.F. Brennan, K. Hess and G.E. Stillman, *Experimental determination of impact ionization coefficients*, *IEEE Electron Device Lett.* **4** (1983) 181.

[5] F. Capasso, W.-T. Tsang and G.F. Williams, *Staircase solid-state photomultipliers and avalanche photodiodes with enhanced ionization rates ratio*, *IEEE Trans. Electron Devices* **30** (1983) 381.

[6] J. Lauter, D. Protić, A. Förster and H. Lüth, *AlGaAs/GaAs SAM-avalanche photodiode: an X-ray detector for low energy photons*, *Nucl. Instrum. Meth. A* **356** (1995) 324.

[7] M. Teich, K. Matsuo and B. Saleh, *Excess noise factors for conventional and superlattice avalanche photodiodes and photomultiplier tubes*, *IEEE J. Quantum Electron.* **22** (1986) 1184.

[8] J.S. Cheong, M.M. Hayat, X. Zhou and J.P.R. David, *Relating the experimental ionization coefficients in semiconductors to the nonlocal ionization coefficients*, *IEEE Trans. Electron Devices* **62** (2015) 1946.

[9] T. Steinhartova et al., *Influence of δ p-doping on the behaviour of GaAs/AlGaAs SAM-APDs for synchrotron radiation*, 2017 *JINST* **12** C11017.

[10] Sentaurus™ Device User Guide, Version L-2016.03, Synopsys, Inc., 700 E. Middlefield Road, Mountain View, CA, USA (2015).

[11] A. Gianoncelli, G. Kourousias, L. Merolle, M. Altissimo and A. Bianco, *Current status of the TwinMic beamline at Elettra: a soft X-ray transmission and emission microscopy station*, *J. Synchrot. Radiat.* **23** (2016) 1526.

[12] R.J. McIntyre, *Multiplication noise in uniform avalanche diodes*, *IEEE Trans. Electron Devices* **ED-13** (1966) 164.

[13] P. Yuan et al., *A new look at impact ionization-part II: gain and noise in short avalanche photodiodes*, *IEEE Trans. Electron Devices* **46** (1999) 1632.